Journal of Controlled Release 285 (2018) 178–186

Contents lists available at ScienceDirect

Journal of Controlled Release

journal homepage: www.elsevier.com/locate/jconrel

Non-invasive tri-modal visualisation *via* PET/SPECT/μCT of recombinant human bone morphogenetic protein-2 retention and associated bone regeneration: A proof of concept

Gry Hulsart-Billström[a,*,1], Ram Kumar Selvaraju[b,1], Sergio Estrada[b], Mark Lubberink[c], Veronika Asplund[b], Kristoffer Bergman[d], Richard Marsell[a], Sune Larsson[a], Gunnar Antoni[e]

[a] Department of Orthopedics, Uppsala University, Uppsala, Sweden
[b] Department of Medicinal Chemistry, Preclinical PET-MRI Platform, Uppsala University, Uppsala, Sweden
[c] Department of Nuclear Medicine & PET, Uppsala University, Uppsala, Sweden
[d] TERMIRA, Stockholm, Sweden
[e] Department of Medicinal Chemistry, Uppsala University, Uppsala, Sweden

ARTICLE INFO

Keywords:
Bone tissue engineering
Hydrogel
Micro computed tomography
Positron emission tomography
Single-photon emission computed tomography
Bone morphogenetic protein 2

ABSTRACT

Bone morphogenetic proteins (BMP's) are vital for bone and cartilage formation, where bone morphogenetic protein-2 (BMP-2) is acknowledged as a growth factor in osteoblast differentiation. However, uncontrolled delivery may result in adverse clinical effects. In this study we investigated the possibility for longitudinal and non-invasive monitoring of implanted [^{125}I]BMP-2 retention and its relation to ossification at the site of implantation. A unilateral critically sized femoral defect was produced in the left limb of rats while the right femur was retained intact as a paired reference control. The defect was filled with a hyaluronan hydrogel with 25% hydroxyapatite alone (carrier control; $n = 2$) or combined with a mixture of [^{125}I]BMP-2 (150 μg/ml; $n = 4$). Bone formation was monitored using micro computed tomography (μCT) scans at 1, 3, 5, 7, 9 and 12 weeks. The retention of [^{125}I]BMP-2 was assessed with single photon emission computed tomography (SPECT), and the bone healing process was followed with sodium fluoride (Na^{18}F) using positron emission tomography (PET) at day 3 and at week 2, 4, and 6. A rapid burst release of [^{125}I]BMP-2 was detected *via* SPECT. This was followed by a progressive increase in uptake levels of [^{18}F]fluoride depicted by PET imaging that was confirmed as bone formation *via* μCT. We propose that this functional, non-invasive imaging method allows tri-modal visualisation of the release of BMP-2 and the following *in vivo* response. We suggest that the potential of this novel technique could be considered for preclinical evaluation of novel smart materials on bone regeneration.

1. Introduction

The growing body of knowledge regarding the mechanisms involved in bone regeneration is enabling the development of a plethora of new biomaterials tailored to promote safe and controlled bone formation in clinical settings. This new generation of smart materials is designed to induce bone regeneration solely by its properties at lowest possible concentration of growth factors with minimum side effects [1–5]. Thus, there is a need for a better understanding of how the *in situ* activity of a smart material correlate with an *in vivo* response. In this context, a non-invasive methodology for visualisation and quantification of the bone healing process would be of great importance.

One such example of a non-invasive technique currently used for the clinical investigation of functional bone imaging is positron emission tomography (PET), along with computed tomography (CT) for anatomical information [6]. PET and sodium [^{18}F]fluoride gives high-resolution PET images and reliable quantification of tracer uptake in bone as a measure of osteoblast activity. [^{18}F]fluoride has the ability to substitute the inorganic components of the bone matrix, namely hydroxide and phosphate, which are found at elevated concentrations at the site of active mineralisation [7,8]. Clinically, [^{18}F]fluoride and PET-CT is often used in the investigation of malignancies in bone tissue [9].

Single-photon emission computed tomography (SPECT) is another clinical modality for bone imaging. SPECT, in contrast to PET, produces a qualitative measure of osteoblastic activity. Ventura et al. compared both techniques for monitoring of bone regeneration by using [^{99m}Tc]

* Corresponding author at: Department of Surgical Sciences, Orthopedics, Uppsala University, Akademiska Sjukhuset Ingång 70 3tr, 751 85 Uppsala, Sweden.
E-mail address: gry.hulsart@surgsci.uu.se (G. Hulsart-Billström).
[1] G. Hulsart-Billström and R. K. Selvaraju contributed equally to this work and should be regarded as joint first authors.

https://doi.org/10.1016/j.jconrel.2018.07.012
Received 30 July 2015; Received in revised form 6 July 2018; Accepted 6 July 2018
Available online 11 July 2018
0168-3659/ © 2018 The Authors. Published by Elsevier B.V. This is an open access article under the CC BY-NC-ND license (http://creativecommons.org/licenses/BY-NC-ND/4.0/).

hydroxymethylenediphosphate in SPECT, and [^{18}F]fluoride in PET. They concluded that PET had a higher sensitivity than SPECT when used in the detection of bone formation [10]. In addition, Ventura et al. explored the use of PET as a method to monitor the *in vivo* response to a calcium phosphate cement that were releasing BMP-2 in a calvarial defect model. They found that there was a positive correlation between the uptake of [^{18}F] fluoride and the volume of *de novo* bone [11].

Computed tomography has been a tool for bone imaging for almost half a century and has since its development by Hounsfield et al. [12] experienced great advances with nano-size resolution imaging and temporal *in vivo* scanning. Bone has been the most common subject of CT scans due to its high density and the field of bone morphometric and bone development is extensively developed and standardised.

Bone regeneration is a complex process that is tightly regulated through the orchestrated release of cytokines. BMP-2 is one of the cytokines produced and released during this process [13,14]. It has strong osteo-inductive effects, which drive the migration of osteoprogenitor cells to the site of bone regeneration, and their subsequent differentiation. These properties demonstrate its high potential as a growth factor, and therefore it is thoroughly investigated as a potential growth factor in combination with scaffolds for regenerative strategies [5,15].

In this proof of concept study, a commercially (TERMIRA) available hydrogel composed of hyaluronan (HA) was used to facilitate bone regeneration. We employed a novel combination of *in vivo* imaging modalities for evaluation of biomaterials, cytokines administered and the *in situ* response to enhance bone regeneration. A critically sized segmental rat femoral defect was used as a temporal *in vivo* model. We fused the methods of Kempen, Ventura, Lienemann and van de Watering [11,16–19] and advanced the technique to apply a tri-modal dual-isotope approach coupling SPECT and PET with traditional μCT validation.

We hypothesise that the combination of PET/SPECT/μCT could be considered for preclinical evaluation of novel smart materials on bone regeneration providing a detailed non-invasive and longitudinal monitoring of bone healing.

2. Materials and methods

Unless otherwise stated, all reagents were purchased from Sigma Aldrich, Stockholm, Sweden.

2.1. Radiolabeling of BMP-2

The radiolabeling was done according to the Hunter and Greenwood method using iodine-125 (I^2) that has a physical half-life of 59.4 days and decays 100% by electron capture [20]. In short, 10 μl of 1,5 mg/ml BMP-2 (InductOs, Medtronic BioPharma, Netherlands) was added to a low binding protein eppendorf tube (VWR, Stockholm, Sweden) followed by 18 μl of (I^2) iodine-125 with an radioactivity of 66,7 MBq 20 μl of Chloramine T (1 mg/ml) (Sigma, No·S-8890, St. Louis, MO, USA) was added to start the reaction. The solution was vortexed for 2 min and 20 μl of sodium metabisulfite (Sigma, No. S-8890, St. Louis, MO, USA) was added to stop the reaction, resuming the vortex mixing for two additional minutes. Phosphate-buffered saline (PBS) was added to a final volume of 500 μl and the solution was transferred to a NAP-5 column (GE Healthcare, Uppsala, Sweden) to separate the [^{125}I]BMP-2 from the free (I^2) [^{125}I]iodine. The column was pre-coated with 1% bovine serum albumin (BSA) in PBS, to minimise the [^{125}I]BMP-2 unspecific binding. To collect the [^{125}I]BMP-2 from the column five repeats of 500 μl of PBS were added to the columns to produce five fractions. The high molecular fraction with the highest activity was used for the study. The [^{125}I]BMP-2 was stored at 4 °C until the preparation of the materials the next day.

2.2. Hydrogel preparation

A commercial hyaluronan aldehyde-poylyvinyl alcohol (HAA/PVAH) system previously described by Bergman et al. was kindly provided by TERMIRA (Auxigel; Termira, Stockholm, Sweden) [9]. In short, the HAA component and PVAH component were dissolved in PBS (pH 7.4) at final concentration 15 mg/ml for HAA and 4.3 mg/ml for PVAH. The HAA were sterilised through a 0.45 μm filter due to its viscous characteristics and PVAH was sterilised through a 0.22 μm filter. The amount of 25% *w/v* of hydroxyapatite powder (Captal, Plasma Biotal, Buxton, UK) with an average particle size of 3.39 μm and Ca/P ratio of 1.67 was sterilised by incubation at 200 °C for 2 h. A 1.5 μg/μl BMP-2 (InductOs, Medtronic, BioPharma, Netherlands) stock solution in formulation buffer (2.5% glycine, 0.5% sucrose, 0.01% polysorbate 80, 5 mM sodium chloride and 5 mM L-glutamic acid, pH 4.5) was prepared according to the manufacturer's instructions. A 2:3 ratio of [^{125}I]BMP-2 (0.03 μg/μl) and BMP-2 (1.5 μg/μl) was mixed, resulting in approximately 2% of the BMP-2 being radiolabeled. The sterile material was used to prepare the HA aldehyde component (15 mg/ml of HAA and 250 mg/ml HAP) and the PVA hydrazide component (2.5 mg/ml PVAH, 250 mg/ml HAP and 0.375 mg/ml BMP-2). The components were loaded into 1 ml syringes at 3:2 volume ratios of HAA and PVAH. The syringes were connected with a sterile adapter and the components were mixed at room temperature (20 °C) back and forth 30 times for 15 s, as previously described [21,22]. As a result, 300 μl of chemically cross-linked hydrogel premix was obtained containing 1% *w/v* polymer, 25% w/v HAP and 0.15 mg/ml [^{125}I]BMP-2, with a radioactivity of approximately 800 KBq.

2.3. Animal model and surgical procedure

The animal study was approved by the Uppsala Committee of Animal Research Ethics (C76/13), according to the Federation of European Laboratory Animal Science Association's guidelines. The hydrogel was injected into a critically sized segmental defect in the (left femur) followed by stabilisation with an external fixator, while the intact right femur was used as paired control for each animal [23]. Male Sprague Dawley (SPRD) rats (400–450 g) were randomised into two groups. The defects were either filled with a control hydrogel carrier ($n = 2$) as it has previously shown no bone formation without addition of growth factors [24,25], or with the hydrogel combined with 30 μg of [^{125}I]BMP-2 ($n = 4$; 80 kBq) at a concentration of 150 μg/ml (~75 μg/kg), which has proven earlier to induce extensive bone formation.

The animals were anesthetised on a facemask with 0.3 l/min oxygen, 1–2.5% isoflurane, and 0.8 l/min nitrous oxide and placed on a 37 °C heat pad during surgery (Isoba vet, Schering-Plough, USA). The left femur was shaved and sterilised with Chlorhexidine Ethanol (5 mg/ml). One dosage of 225 mg/kg antibiotics (Zinacef, GlaxoSmithKline AB, Sweden) was given subcutaneously. The femur was exposed by making a longitudinal lateral skin incision followed by blunt dissection in-between m. vastuslateralis and m. biceps femoris. Four 0.75 mm bicortical holes were drilled (Dremel multi, Robert Bosch Tool Corporation, Germany) by placing a guide on the lateral side of the femur that was centred mid-diaphyseal using a purpose-built forceps. Each drill hole was tapped followed by insertion of 1 mm stainless steel pins. The pins were pierced through the skin and locked into an aluminium and stainless steel external fixator. An oscillating saw (Stryker total performance system, TPS sagittal saw with 5 mm saw blade) was used to create a 5 mm mid-diaphyseal defect guided by a saw guide to standardise the defect. Saline was administered to prevent tissue necrosis during the sawing. The resected bone was extracted with a clamp and debris was washed out of the defect with saline. Two sutures (Polysorb, Tyco Healthcare, Gosport, UK) were applied in the fascia layer, with the proximal left untied. The volume of 200 μl of hydrogel with a radioactivity of approximately 600 KBq and a dose of 30 μg of BMP-2 was injected into the defect, after which the second fascia (4-0

resorbable, Polysorb, Tyco Healthcare, Gosport, UK) was tied to close the bone defect compartment. The wound was closed subcutaneously and inversed transcutaneously. The defects were either filled with hydrogel alone ($n = 2$) or with hydrogel + [^{125}I]BMP-2 ($n = 4$). For analgesia 0.05 mg/kg buprenorphine (Temgesic, Sheringer Plough, Brussels, Belgium) was administered subcutaneously twice daily for 3 days. Free load bearing was allowed.

2.4. In vivo imaging

2.4.1. μCT

The rats were examined by μCT (SkyScan 1176, Kontich Belgium) post-surgery and at weeks 1, 3, 5, 7, 9 and 12, using source voltage: 90 kVp; current150 mA: pixel size 36 μm filter: 0.1 mm^3; exposure time: 150 ms; frame averaging: 1; rotation step: 0.70; field of view: 68 mm. The μCT settings were optimised to minimise the radiation dose to the animals without compromising the quality of the data analysis. The anesthetised animal (isoflurane 1.0%–2.5% in 50%/50% medical oxygen: air at 450 ml/min) was placed on a gantry bed heated through hot air to prevent hypothermia. The NRecon software was used for reconstruction. A 3 mm volume of interest was set in the middle of the defect as reference point to exclude the shaft of the femurs. Software CTAn was employed for analysis while CTvox was applied for bone imaging; all software's were from SkyScan, Bruker, Kontich, Belgium.

2.4.2. CT/SPECT/PET

The animals were scanned in Triumph™ Trimodality System (TriFoil Imaging, Inc., Northridge, CA, USA) after three days, and at weeks 2, 4, and 6 post surgery. The anesthetised animal (isoflurane 1.0%–2.5% in 50%/50% medical oxygen: air at 450 ml/min) was placed on a heated gantry bed to prevent hypothermia and taped to prevent large movements during the study. The breathing rate was continuously monitored with integrated sensors. CT examination was performed using an 8 cm field of view, only for anatomical correlation to confirm the animal position in the scanner with following settings; voltage: 80 kVp; current: 130 mA; exposure time: 133 s.

Next, a SPECT examination (75A10 collimators, acquisition over energy peak of 27 KeV) was performed over the same position for 30 min (32 projections, 56 s/projection). Sequentially, a dynamic PET scan over same position as in the SPECT was performed in list mode for 30 min, starting with the single bolus injection of [^{18}F]fluoride, (provided from PET Centre at Uppsala University Hospital) at a dose of 53.94 ± 6.09 MBq/kg with a molar activity in the range 200–600 GBq/μmol in a maximum volume of 500 μl, *via* the tail vein catheter. The animals were allowed to wake up after scans under supervision and housed under standard laboratory conditions with free access to laboratory animal food and water.

2.4.3. Image analysis

The CT raw files were reconstructed using Filter Back Projection. SPECT raw data was reconstructed by an ordered Subset Expectation Maximisation iterative reconstruction algorithm (8 subsets and 5 iterations) in FLEX SPECT software. PET raw data were reconstructed into 20 frames (12 × 10s, 3 × 60s, and 5 × 300 s) using maximum-likelihood expectation maximisation 2-dimensional algorithm, algorithm (10 iterations, 2 subsets). Reconstructed PET images had voxel values of (0.5, 0.5, 0.175) mm in X, Y & Z axis.

SPECT–CT and PET-CT data were fused and analysed in PMOD 3.510 (PMOD Technologies Ltd., ZRH, Switzerland). Regions of interest (ROIs), radius (r) = 3 mm, were drawn on fused PET-CT image (Fig. 1), along transaxial view. ROIs were drawn over 4–7 consecutive sections to define volume of interest (VOI) in legs (Fig. 1 A). Both the femur with fracture and the healthy contralateral femur had VOIs drawn (Fig. 1 B); within the fracture femur 3 cylindrical VOIs (4 × 0.175 mm), one VOI over each external-fixator pin hole site *i.e.*, at hip (Pin_hip) and knee (Pin_knee), and a VOI over the defect (Frac_leg) were drawn (Fig. 1C) to

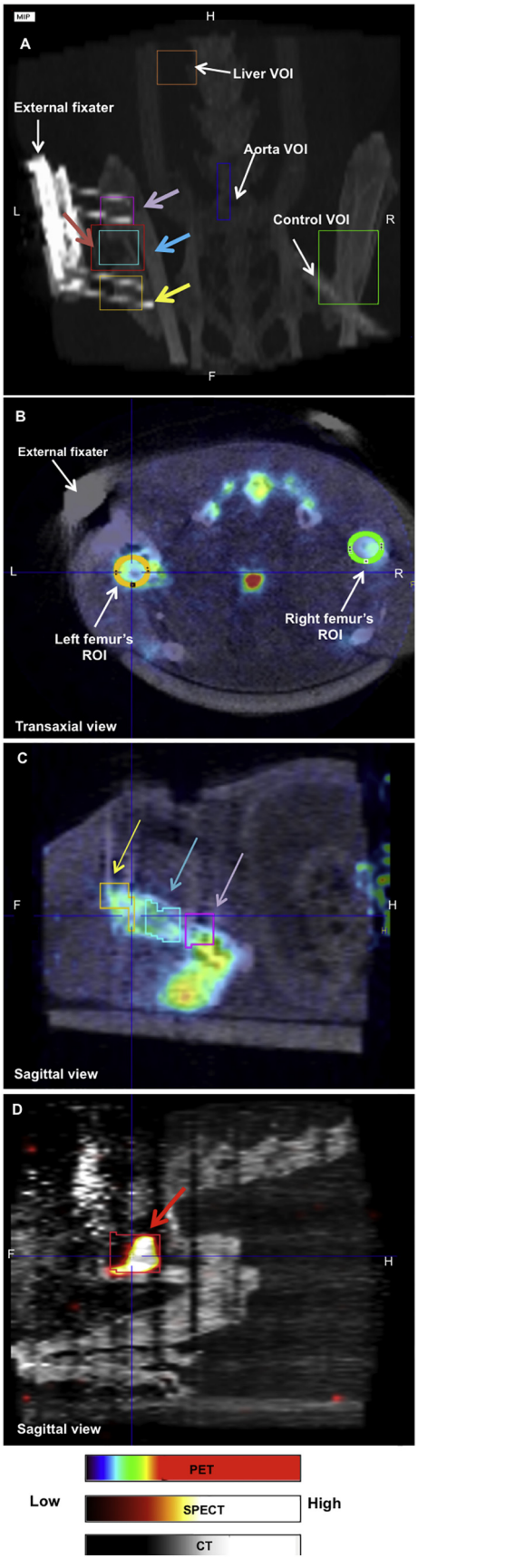

(caption on next page)

Fig. 1. Illustration of the ROIs and the VOIs that were used to analyse dynamic [^{18}F]Fluoride-PET images and [^{125} I]BMP-2 release.
(A) Maximum intensity projection (MIP) of CT image, coronal view, shows complete set of VOI's drawn in the analysis. Fracture leg parts (left femur), namely, pin_knee (purple), Frac_leg/defect (cyan), BMP-2 lump (red) and pin_hip (yellow); control right femur (green), Liver (orange), and Aorta (blue). (B) Transaxial section of fused [^{18}F]Fluoride-PET-CT image show ROI (Ø = 6 mm drawn over right femur (control) and left femur (frac_leg). (C) Fused PET-CT image, sagittal view of the same section as (B) with VOI's over left femur. PET is represented in RGB. (D) 3 days post surgery. Fused SPECT-CT image (MIP), sagittal view. Arrow points at [^{125} I]-BMP-2. SPECT in presented hot iron colour. Abbreviations (orientations): H-head, F- foot. L-left. R-right.

estimate the [^{18}F]fluoride uptake at hydrogel site and to prevent cross fire effect from external-fixator pin hole points. Uptake in liver (orange VOI) was used create SUV scale for comparison of PET images between principle and control. Liver VOI was a copy of Frac_leg VOI (cyan), hence were of same volume. PET data are presented as net influx constant (ki) of [^{18}F]fluoride obtained from Patlak analysis, using an aortic VOI (4–5 pixels in 5–7 consecutive sections) as the input function.

For SPECT studies, a separate VOI (red) was drawn (radius (r) = 5 mm) over the fracture leg (Fig. 1 D) as a post-operative reposition of the hydrogel was observed in the defect. SPECT data were presented as percentage of retained [^{125}I]BMP-2 compared to initial scan in Fig. 4 (Fig. 4A, D, G, J) and as total counts (total counts per min * volume) in Fig. 5A.

3. Results

3.1. Radiolabeling

The radiochemical yield of [^{125}I]BMP-2 was about 60% based on the starting amount of iodine-125. It was important to coat the NAP-column with BSA to avoid that BMP-2 would adhere to the column surface [26,27]. We collected the high molecular fractions from the column and assumed that the radioactivity from this column was BMP-2 labelled with iodine-125. The assumption was confirmed by the similarity of the release profile determined by ELISA assay [3]. Estimated molar activity of [^{125}I]BMP-2 was 0.3 GBq/μmol. Sodium [^{18}F]fluoride was obtained by standard procedure by bombardment of oxygen-18 water with 17 MeV protons, ^{18}O(p,n)^{18}F, followed by separation on an ion exchange resin and formulation in a mixture of 0.1 M phosphate buffer pH 7.4/saline.

3.2. Animal model

Two out of four animals in the hydrogel + BMP-2 group could be followed through the whole experiment until week 12. The two others rats had loosening of a pin and were euthanised immediately, in order to diminish any suffering of the animal. One rat had pin failure at week 6 [rat 4] and was euthanised before the appointed PET scan, the other at week 9 [rat 2]. One of the rats that were followed through the whole 12-week period failed to be scanned at week 4 due to a breakdown of the PET scanner during scanning [rat 1]. Both controls experienced pin loosening of a pin at week 9 and were euthanised immediately.

3.3. μCT

Bone volume and tissue volume was measured using μCT. Bone formation was first observed at week 3 in the hydrogel + BMP-2 group (n = 4; mean = 7.5 ± 1.17 mm^3) (Figs. 2 and 3). The hydrogel + BMP-2 group continued to increase in bone volume over time with 15.3 ± 4.43 mm^3 (n = 4) at week 5 (Fig. 2a), no change at week 7 (14.3 ± 1.63 mm^3, n = 4), then again an increase at week 9 with 19.55 ± 6.39 mm^3 (n = 3) and week 12 with a range of 20.36–21.59 mm^3 (n = 2). One rat in the hydrogel + BMP-2 group was euthanised at week 6 during PET scan and another at week 9 due to problems with the external fixator. The control hydrogel reached its maximum bone volume at week 3 (n = 2; range = 0.56–0.22 mm^3) and decreased until week 7 where no bone was detected (Fig. 2a). One of the control rats was euthanised after week 9 due to loosening of the pins in the external fixator and the other was euthanised after week 12 and excluded from the CT analysis due to failure of the external fixator, which could not separate the bone shafts, the image is presented in Fig. 3. The density thresholds for the total VOI volume here mentioned as tissue volume according to bone ASBMR nomenclature, included the hydrogel, which was radiopaque because of the 25% of hydroxyapatite, giving similar start values of tissue volume in the hydrogel + BMP-2 and the hydrogel alone groups at scan 1. Over time, the hydrogel degraded and the tissue volume decreased in the hydrogel alone group. The opposite response was seen, in the hydrogel + BMP-2 group, where the hydrogel was replaced by newly formed bone (Fig. 2b). The replacement could be described by the ratio of tissue volume/bone volume where the replacement of hydrogel to bone was observed in the hydrogel + BMP-2 (Fig. 2c). The μCT images of the hydrogel + BMP-2 and the controls revealed that the material was visible for the first week. At week 3 callus formation was noticed in the hydrogel + BMP-2 group and dense tissue was also visible in the hydrogel alone group although this dense tissue disappeared over time. In contrast, *de novo* bone accumulated in the hydrogel + BMP-2 group through the whole observation period (Fig. 2–3), which were later confirmed macroscopically (Suppl. Fig. S1).

3.4. PET

Osteoblast activity was examined by [^{18}F]fluoride uptake, which was measured by the net influx rate constant (K_i, the overall net rate of [^{18}F]fluoride uptake) assessed by PET. At the first scan (day 3) similar level of uptake was detected in all samples with no difference between hydrogel, hydrogel + BMP-2 or intact contralateral controls (< 0.05 ml/cm^3/min). At the second scan (2 weeks), an increase was detected in both the hydrogel + BMP-2 group (0.44 ± 0.09 ml/cm^3/min (n = 4)) as well as for the two hydrogel-alone femora, (range = 0.26–0.34 l/cm^3/min (n = 2)). At week 4, a continuous increase was seen in the hydrogel + BMP-2 group with a K_i of 0.59 ± 0.40 (n = 3) the Hydrogel group had a K_i range of 0.10–0.13, (n = 2). The PET images revealed a strong osteoblast activity at the site of the defect in the hydrogel + BMP-2 group, whereas the Hydrogel group mainly showed activity at the site of the pinholes (Figs. 4 and 6), a VOI was placed over the pin holes in order to register the amount of activity at this site of the pin holes, which could lead to a possible spill over effect registered in the adjacent defect VOI. The pinholes did induce an elevated activity, which was seen in both groups (Fig. 4). There was still a tenfold increase of K_i in the hydrogel + BMP-2 group at week 6 (0.38 ± 0.06 ml/cm^3/min (n = 2)) compared to contralateral bone.

PET images are presented in relative SUV scale (SUVR = 15) with respect to liver. Uptake of [^{18}F]fluoride in liver was similar in principles (50.361 ± 10.808 kBq/cc) and controls (51.828 ± 6.990 kBq/cc). Liver was used as reference tissue and PET images were normalised to SUVR 15, in other words, $SUV_{Frac\ leg}/SUV_{Liver}$ = 15.

3.5. SPECT

In vivo [^{125}I]BMP-2 (≈600 kBq) retention was monitored by SPECT. The hydrogel + BMP-2 had a rapid release between day 3 and 2 weeks, followed by a slower release during the following 2 weeks (Figs. 4 and 5) SPECT images showed a fast clearance of [^{125}I]BMP-2 from the site of implantation. Although, a small amount (0.17 ± 0.18 (counts/min) * volume) of retained [^{125}I]BMP-2 was still visible at week 4 (Figs. 4–6).

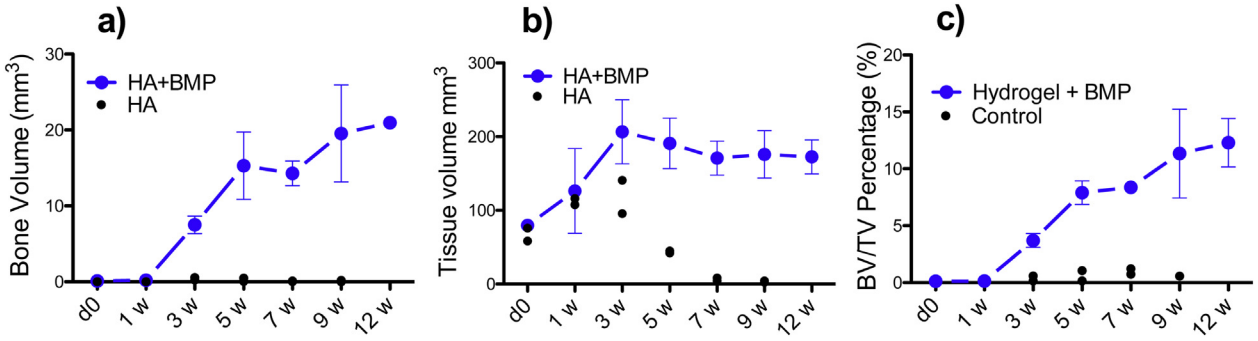

Fig. 2. (a) Bone volume, (b) tissue volume (c) and bone volume fraction, for the two groups, hydrogel alone (displaying each replicate) or hydrogel + BMP-2 (mean ± SD), as assessed by μCT.

4. Discussion

In this study, we present a novel combination of *in vivo* modalities for evaluation of biomaterials and cytokines administered to enhance bone regeneration. A segmental femoral bone defect in a rat model proved suitable for the aim, due to its ability to retain the biomaterial at the site of injury. Thus enabling a longitudinal analysis of biomaterial replacement, cytokine retention, and the associated bone regeneration using a tri-modal dual-isotope approach combining SPECT, PET and μCT.

The choice of biomaterial to develop this proof of concept was a HA hydrogel that has been well characterised in earlier publications, demonstrating numerous advantageous properties, as further discussed below.

HA is a non-immunogenic, highly inter-species conserved molecule which, when loaded with BMP, has been successfully used to promote orthotopic and ectopic bone formation [22,24,25,27–30]. HA is a glycosaminoglycan that can be derived from E Coli. This recombinant form does not possess any immunogenic properties, contrary to the currently available bovine-derived collagens, which can also be used as carriers of BMPs. HA has several cell binding motifs, including CD44 (a mesenchymal stem cell receptor) and intercellular adhesion molecule-1 (involved in cell motility), which makes the material an attractive platform for cell-adhesion and proliferation. Native HA has a rapid degradation rate, with a turnover of > 10 mg per day in humans [31,32].

The HA hydrogel has earlier proven to release BMP-2 rapidly during the first week followed by a slower release for the remaining 3 weeks in a rat ectopic model where the thigh muscles were examined *ex vivo* in a gamma counter [27]. This kind of biphasic release profile can facilitate the migration of osteoprogenitor cells from the periosteum and bone marrow [33–36] and the benefits of a burst release of BMP-2 from carriers has been confirmed previously [34]. Interestingly, the same initial burst of BMP signalling is evident in normal healing of fractures. Marsell et al. showed an early peak of BMP-2 mRNA expression within the first 24 h after reaming of a rat tibia, followed by a later peak after

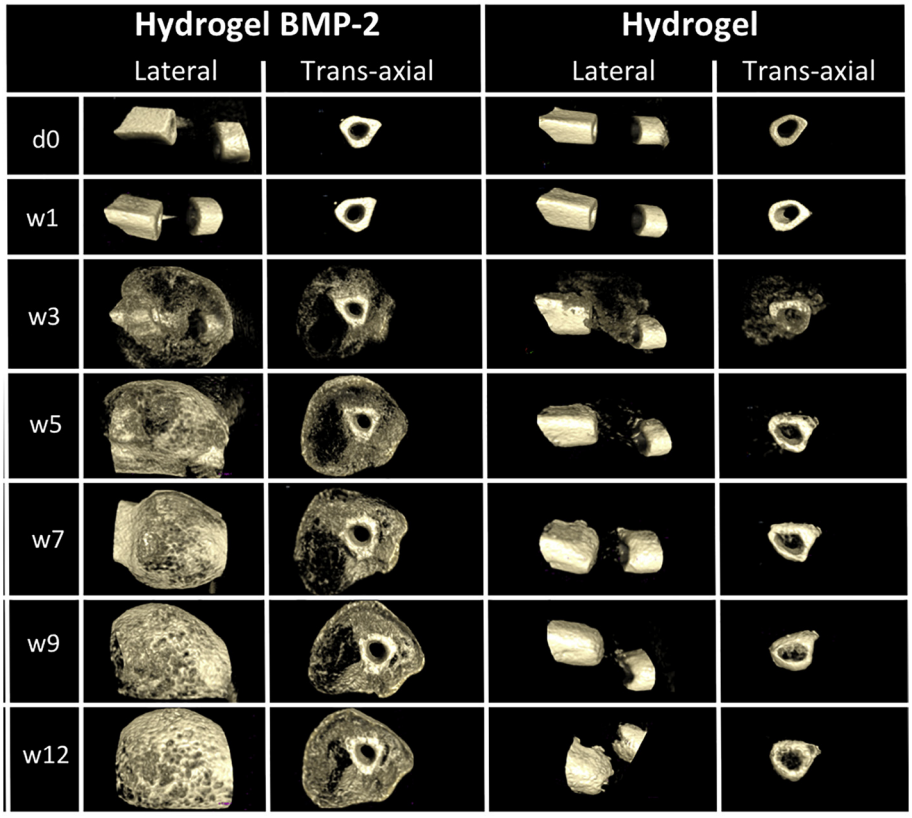

Fig. 3. Representative μCT images of femoral defects filled with hydrogel + BMP-2 at post surgery and at weeks 1, 3, 5, 7, 9, and 12.

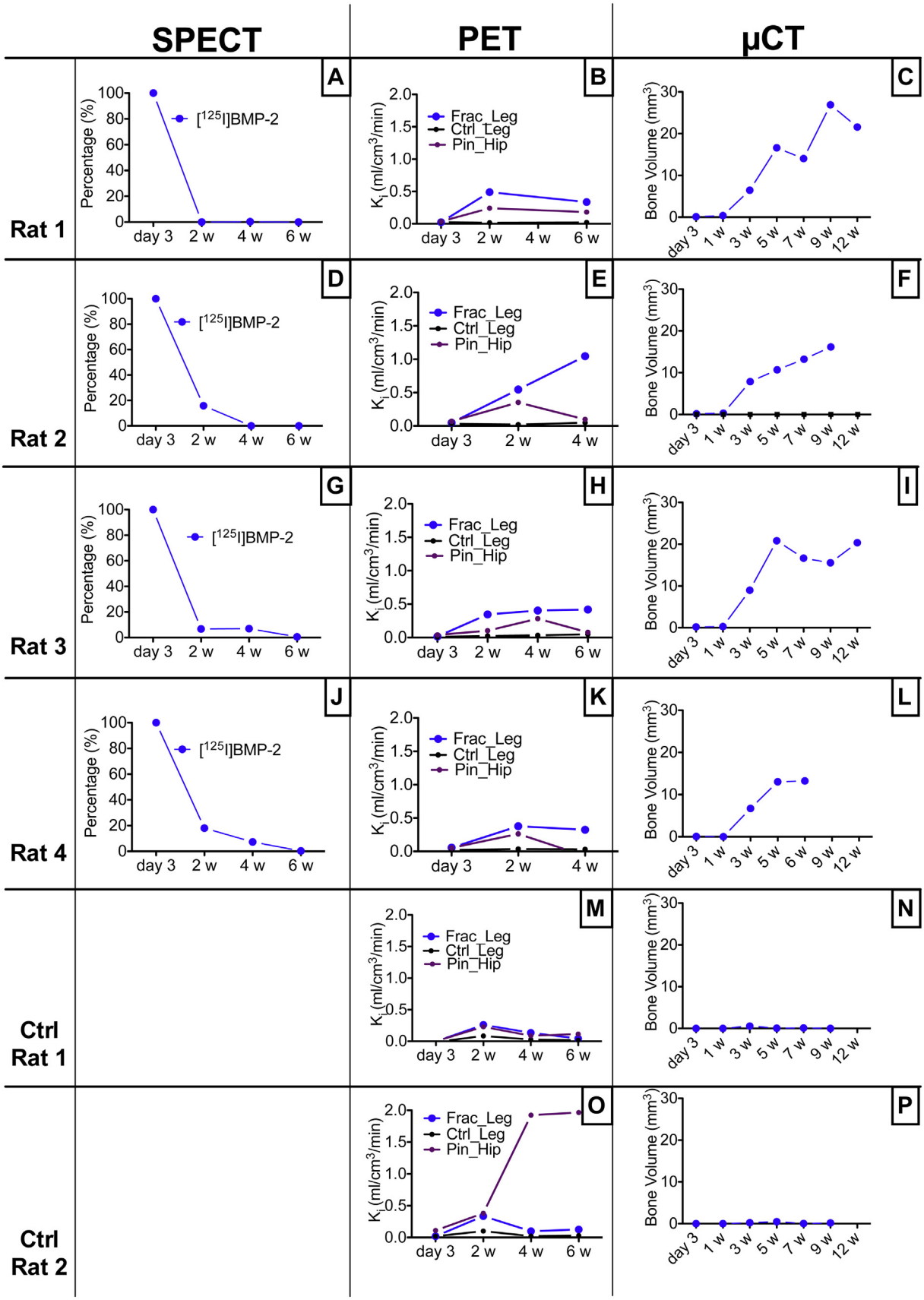

Fig. 4. Comparison of [^{125}I]BMP-2 retention (SPECT; A, D, G, J), osteoblast activity (PET; B, E, H, K, M, O) and bone formation (μCT; C, F, I, L, N, P) in femoral defects of principals (rat 1–4) and controls (1–2). (Frac_Leg = defect (blue), Ctrl_Leg = healthy contralateral leg (black), Pin_hip = Proximal pinhole site (purple).) (For interpretation of the references to colour in this figure legend, the reader is referred to the web version of this article.)

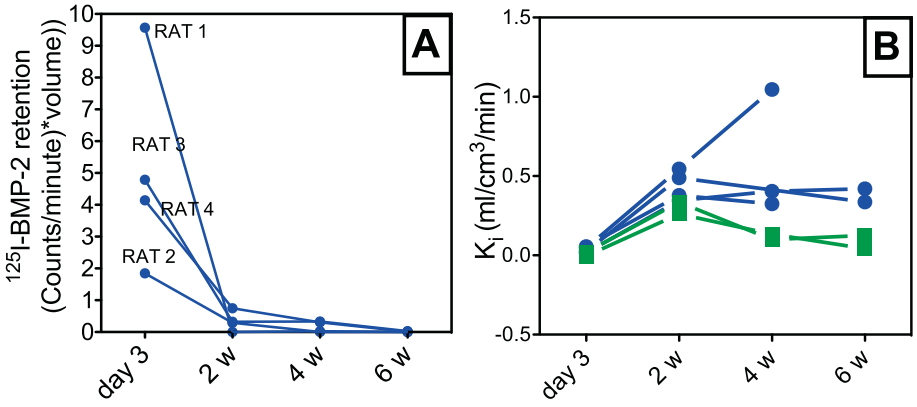

Fig. 5. [^{125}I]BMP-2 retention measured by SPECT (A) and [^{18}F]fluoride uptake (B) measured as K_i the defect leg and the healthy control. Each individual value is represented in the graph. a) The hydrogel + BMP-2 had a rapid initial release between day 3 and 2 weeks where most of the [^{125}I]BMP-2 was released. A small amount of retained [^{125}I]BMP-2 was still visible at week 4. b) [^{18}F] fluoride uptake for each individual rat (blue = principals, green = controls). (For interpretation of the references to colour in this figure legend, the reader is referred to the web version of this article.)

7 days. Intriguingly, BMP-2 mRNA expression was not only induced in endosteal lining cells, cortical osteocytes and periosteal cells of the reamed bone, but also in the contralateral bone that showed a BMP-2 mRNA peak 7 days after the reaming [36]. The systemic response could cause a positive effect on the [^{18}F]fluoride uptake of the contralateral bone.

The critical sized segmental defect model was chosen because of the estimation of low osteoblast activity in the controls and that the volume of the defect would be sufficient to detect the implanted [^{125}I]BMP-2 in the preclinical CT/SPECT/PET camera. The defect size should be large enough to reduce the partial volume effect. The defect model itself proved suitable for imaging the material, although the metal external fixator created artefacts in the CT/SPECT/PET. In addition, the study period of 12 weeks was acceptable for the hydrogel + BMP-2 treated groups as the defect healed and the *de novo* bone provided satisfactory stability of the femur. This did not apply for the control group where the external fixators fatigued and failed over time. These findings emphasise and validate the segmental defect model as a critically sized defect model. Retrospectively, shorter periods between scans during the first weeks to observe the initial release of [^{125}I]BMP-2 would have been beneficial. Also, a shorter total study time could have been sufficient. In this study the duration of the scans were up to 1.5 h in the CT/SPECT/PET, which affected the animals negatively, especially at the early time period after surgery. Hence, the ethical impact of scanning more frequently must be carefully considered against the potential benefit gained from the additional data.

The BMP-2 release from this cross-linked HA was previously investigated through the use of radio-iodinated growth factor in an ectopic rat model [27]. There, the HA-hydrogel with radiolabelled BMP-2 was implanted intramuscularly in the thigh muscle. The rats were euthanised at different time points and their limbs were examined *ex vivo* in a gamma counter. This preceding study provided accurate measurements of the retained BMP-2 at the site of administration. However, the use of *ex vivo* measurements led to the need for an excessive use of animals and to individual variation between the time points [27], which inspired us to develop the current tri-modal combination. The combination of SPECT/PET/μCT provided a detailed non-invasive longitudinal monitoring of bone healing and direct correlation to [^{125}I]BMP-2 retention at the application site with the inherent advantage of reducing the number of animals and eliminating the individual variation between the time points by using each animal as its own control. The presence of the radiolabeled BMP-2 could be visualised by SPECT and rapid release was monitored between day 3 and 2 weeks post-surgery, followed by a slow decrease of the [^{125}I]BMP-2 retention until

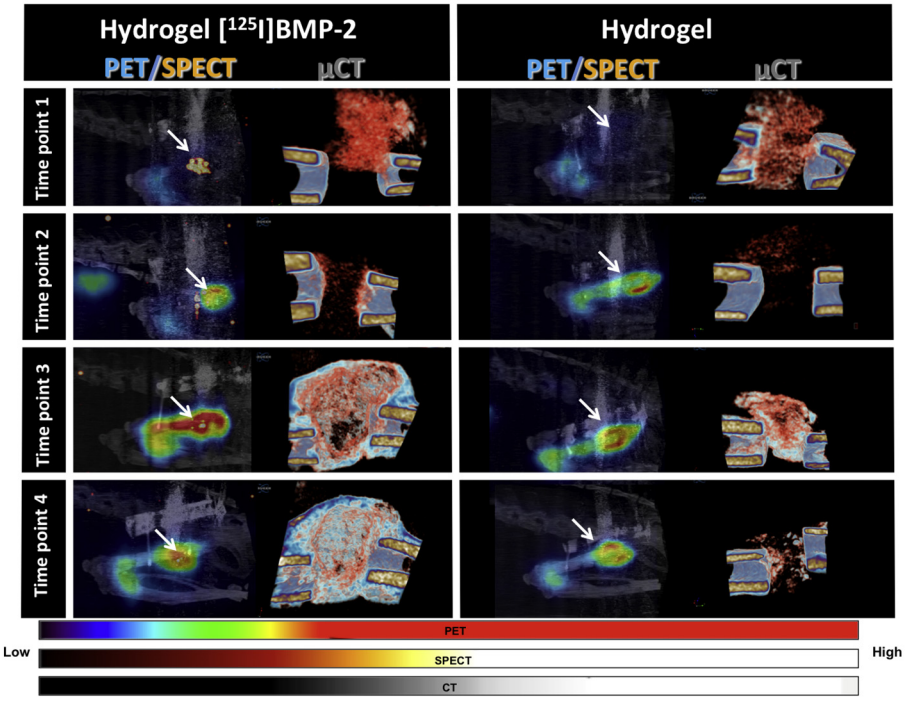

Fig. 6. Representative co-registered SPECT/PET/CT images of osteoblast activity in femoral defects (white arrow) filled with hydrogel + BMP-2 at day 3, week 2, 4 and 6 in a segmental femoral defect. μCT images display the bone formation in progress in close time frame to the PET/SPECT imaging. μCT scans were undertaken at day 0 and week 1, 3, 5, 7, 9 and week 12. The threshold of the image was set to include low densities in order to display the material post-surgery. PET images are presented in RGB colours as SUVR 15. Whereas, SPECT (hot iron) and CT (gray) are presented as maximum intensity projections in arbitrary units.

week 4. In previous work, the authors excised and measured the iodine-125 radioactivity in all organs, including the thyroid, to confirm that the iodine-125 radioactivity was not from free [^{125}I]iodide but still bound to the BMP-2 molecule. Since very small amounts of iodine-125 could be measured in the thyroid we concluded that released radioactivity most likely was in the form of [^{125}I]BMP-2 [27].

During the same period, the *in vivo* response, measured as an increased rate influx constant, defined as uptake of [^{18}F]fluoride, was observed at the site of the defect using PET. This was first observed in the PET scan, two weeks after surgery and with a peak [^{18}F]fluoride uptake at week 4. A continuous uptake was seen at the site of the pinholes for the external fixator (Figs. 4–6). This is probably due to the mechanical stimuli from the external fixator. Our results corroborate earlier findings by Ventura et al., where the uptake of [^{18}F]fluoride in calvarial defects was investigated after treatment with calcium phosphate cement discs soaked in 10 μg of BMP-2. Even though the materials are very different from each other, a similar release profile of BMP-2 between the cement and the hydrogel was described [11]. The [^{18}F]fluoride uptake in the current study seemed to be directly proportional to bone regeneration as observed *ex vivo* (Suppl. Fig. S1). SPECT and PET studies were analysed until a visible fraction of ^{125}I-BMP-2 was observable in SPECT, to follow the BMP-2 retention and its influence on bone regeneration *via* [^{18}F]fluoride. There was no evident signal at week 6, implying no traces of BMP-2 at the site of surgery to boost bone regeneration. Therefore, the functional imaging was terminated after the week 6 acquisitions. However, further analysis of bone regeneration with μCT was continued to evaluate any differences in bone volume between BMP-2 induced- and natural bone regeneration.

Numerous groups have confirmed that the uptake of [^{18}F]fluoride is associated with the concentration of bone-forming minerals, suggesting biomineralisation to be the sole responsible factor for the radiotracer's uptake [37–39]. Some have investigated the correlation between [^{18}F]fluoride uptake to the formation of *de novo* bone at specific sites seen in histomorphometry. Li et al. used high-resolution PET and [^{18}F]fluoride to detect micro damage due to mechanical stress *in vivo* and co-localised it with the damage detected by histology and autoradiography. The spots seen in PET corresponded to the *in vitro* autoradiography that showed accumulation of radioactive tracer that later were verified as micro cracks by microscopy [37]. The same specificity was seen in parathyroid hormone (PTH) treated osteoporotic women where PET detected higher rate of bone formation in cancellous bone, corresponding with the action of PTH, which prolongs the life and activity of present osteoblasts [39]. PET was also tested as a complement to CT in a clinical study to evaluate and visualise the vascularisation and bone formation around allografts in cemented total hip replacements, since the high density of the implant can hamper the CT of the allograft, giving no difference between the allograft and newly formed bone. In agreement with *in vivo* studies, an early response in terms of increased blood flow, and bone formation adjacent to the allograft was detected already at day 8 post-surgery with comparable levels to the contralateral bone first seen after one year [8]. These studies suggest PET as a preferential and reliable method to understand bone anabolism and [^{18}F]fluoride uptake is indeed a measure of bone regeneration in both preclinical and clinical settings.

The inorganic part of bone is composed of trace elements with the chemical formula described as $(Ca, Na, Mg)_{10}(PO4, HPO4, CO3)_6(OH, Cl, F)_2$ [40]. Excessive systemic exposure to fluorides can disrupt bone homeostasis resulting in changes to gene expression, cell stress, and cell death [41]. Fluoride has been used for control of crystal size and has demonstrated interference with bone formation in a dose-dependent manner [29,42]. In the current study, the dose of fluoride injected (53.94 ± 6.09 MBq/kg) at each scan was negligible due to the high molar activity (approximately 400 GBq/μmol). The animals were investigated with [^{18}F]fluoride at 4–5 occasions and the estimated total amount of fluoride administered was < 7 ng. Thus, well below the detection limit for any effect on the bone healing process and insignificant in relation to fluoride concentrations of drinking water.

The animals were exposed to radiation from all three methods. The [^{125}I]BMP-2 protein, [^{18}F]fluoride and X-rays from both the CT and μCT scanners could affect the well being of the animals. Excessive radiation of bone leads to decrease in vascularisation and in cellularity [43]. It is therefore very important to control and plan the study to minimise the number of scans. We estimated the radiation dose to keep the total exposure for each animal under 1 Gray, which is a critical dose of radiation [44,45].

The objective for this proof of concept study was to develop a method that could be used for future monitoring and visualisation of biomaterial performance *in vivo*. The feasibility of the method could be demonstrated with the usage of 4 rats in the hydrogel + BMP-2 group and 2 rats as controls, all in accordance to the 3Rs [46]. Evidently, there are limitations to the current study. Considering humane *versus* experimental end point, some subjects had to be sacrificed earlier than planned. Thus, we chose not to perform statistical analysis due to the small number of samples. According to power calculations $n = 7$ repetitions per group would be necessary to obtain statistically significant data. Furthermore, the acquisition time of the PET scan (30 min) was relativity short for this type of analysis. This was a compromise in order to ensure that the animals remained healthy for continuous scans. This limitation was of minor significance, as the uptake of [^{18}F]fluoride depends both on bone blood flow and on osteoblastic activity. Additionally, μCT data were used to further strengthen the conclusion rather than solely depending on the PET data.

Interestingly, this method revealed, in the controls, an initiation of a healing process at week 2 and 4, with elevated [^{18}F]fluoride uptake, confirmed by a display of denser tissue in μCT at week 3 (Figs. 2b, 3 and 6). As expected, healing of the controls failed and dense tissue was absent at week 4. To the authors' knowledge, this is the first time the start of a healing process in an empty critical size defect has been detected, which emphasises the importance of sequential models.

The ability to reveal temporal events of the biomaterials *in situ* is the most obvious advantage of this tri-modal *in vivo* model. Henceforth this method will be employed to monitor growth factor retention of tuneable smart materials [3,47], implementing comparative studies with sample numbers estimated by power calculus.

In our current investigation, a rapid burst release of the [^{125}I]BMP-2 was observed from the hydrogel + BMP-2, which would have required shorter time frames between the first scans to be able to adequately observe the [^{125}I]BMP-2 release of this particular material. However, the time points were suitable for observing the *in vivo* response to the material by PET, demonstrating an elevated uptake of [^{18}F]fluoride between week 2 and 6, with mineralisation depicted in the CT, proportionate to the uptake of fluoride observed in the PET studies. From this study, it was clear that a compromise is needed between the use of enough time points to be able to follow the release profile of the material and at the same time keep the radiation dose to a minimum. The potential use of this model in clinical settings can be discussed, but this *in vivo* preclinical model can be used to identify the optimal timing for effective delivery of osteogenic factors and to visualise the *in situ* action of selected biomaterials.

5. Conclusion

We have developed a functional, non-invasive imaging method that allowed visualisation of the *in vivo* release of [^{125}I]BMP-2 using SPECT and the subsequent *in vivo* response, as measured with [^{18}F]fluoride-PET and μCT, in terms of bone regeneration. This double-isotope approach with tri-modal visualisation could be highly applicable in several disciplines in regenerative medicine allowing a temporal monitoring of biomaterials' *in situ* action. We suggest that the potential of this novel technique should be considered for preclinical evaluation of novel smart materials for bone regeneration.

Acknowledgement

The research leading to these results received funding from European Community's Seventh Framework Programme European Community Seventh Framework Programme Grant, BioDesign (262948). We would like to thank Britt-Marie Andersson for valuable help and technical support. Olof Eriksson for valuable help with SPECT, as well as Ines Moreno, Vitali Gorinov, Edoardo Scarpa, Su-Yin Lim and Cecilia Persson for constructive comments on the manuscript.

Appendix A. Supplementary data

Supplementary data to this article can be found online at https://doi.org/10.1016/j.jconrel.2018.07.012.

References

[1] A.J. Engler, S. Sen, H.L. Sweeney, D.E. Discher, Matrix elasticity directs stem cell lineage specification, Cell 126 (2006) 677–689.
[2] M.J. Dalby, A. Andar, A. Nag, S. Affrossman, R. Tare, S. McFarlane, R.O. Oreffo, Genomic expression of mesenchymal stem cells to altered nanoscale topographies, J. R. Soc. Interface 5 (2008) 1055–1065.
[3] G. Hulsart-Billstrom, P.K. Yuen, R. Marsell, J. Hilborn, S. Larsson, D. Ossipov, Bisphosphonate-linked hyaluronic acid hydrogel sequesters and enzymatically releases active bone morphogenetic protein-2 for induction of osteogenic differentiation, Biomacromolecules 14 (2013) 3055–3063.
[4] D.M. Gibbs, C.R. Black, J.I. Dawson, R.O. Oreffo, A review of hydrogel use in fracture healing and bone regeneration, J. Tissue Eng. Regen. Med. 10 (2016) 187–198.
[5] K. Schmidt-Bleek, B.M. Willie, P. Schwabe, P. Seemann, G.N. Duda, BMPs in bone regeneration: less is more effective, a paradigm-shift, Cytokine Growth Factor Rev. 27 (2016) 141–148.
[6] J. Czernin, N. Satyamurthy, C. Schiepers, Molecular mechanisms of bone 18F-NaF deposition, J. Nucl. Med. 51 (2010) 1826–1829.
[7] T. Aoba, Y. Shimazu, Y. Taya, Y. Soeno, K. Sato, Y. Miake, Fluoride and apatite formation in vivo and in vitro, J. Electron Microsc. 52 (2003) 615–625.
[8] J. Sorensen, G. Ullmark, B. Langstrom, O. Nilsson, Rapid bone and blood flow formation in impacted morselized allografts: positron emission tomography (PET) studies on allografts in 5 femoral component revisions of total hip arthroplasty, Acta Orthop. Scand. 74 (2003) 633–643.
[9] J.D. Oldan, A.S. Hawkins, B.B. Chin, (18)F sodium fluoride PET/CT in patients with prostate cancer: quantification of normal tissues, benign degenerative lesions, and malignant lesions, World J. Nucl. Med. 15 (2016) 102–108.
[10] M. Ventura, G.M. Franssen, E. Oosterwijk, O.C. Boerman, J.A. Jansen, X.F. Walboomers, SPECT vs. PET monitoring of bone defect healing and biomaterial performance in vivo, J. Tissue Eng. Regen. Med. 10 (2016) 843–854.
[11] M. Ventura, O.C. Boerman, G.M. Franssen, E. Bronkhorst, J.A. Jansen, X.F. Walboomers, Monitoring the biological effect of BMP-2 release on bone healing by PET/CT, J. Control. Release 183 (2014) 138–144.
[12] G.N. Hounsfield, Computerized transverse axial scanning (tomography). 1. Description of system, Br. J. Radiol. 46 (1973) 1016–1022.
[13] M.R. Urist, Bone: formation by autoinduction, Science 150 (1965) 893–899.
[14] J.M. Wozney, V. Rosen, M. Byrne, A.J. Celeste, I. Moutsatsos, E.A. Wang, Growth factors influencing bone development, J. Cell Sci. Suppl. 13 (1990) 149–156.
[15] D. Gothard, E.L. Smith, J.M. Kanczler, H. Rashidi, O. Qutachi, J. Henstock, M. Rotherham, A. El Haj, K.M. Shakesheff, R.O. Oreffo, Tissue engineered bone using select growth factors: a comprehensive review of animal studies and clinical translation studies in man, Eur. Cell Mater. 28 (2014) 166–207 (discussion 207-168).
[16] D.H. Kempen, M.J. Yaszemski, A. Heijink, T.E. Hefferan, L.B. Creemers, J. Britson, A. Maran, K.L. Classic, W.J. Dhert, L. Lu, Non-invasive monitoring of BMP-2 retention and bone formation in composites for bone tissue engineering using SPECT/CT and scintillation probes, J. Control. Release 134 (2009) 169–176.
[17] F.C. van de Watering, J.D. Molkenboer-Kuenen, O.C. Boerman, J.J. van den Beucken, J.A. Jansen, Differential loading methods for BMP-2 within injectable calcium phosphate cement, J. Control. Release 164 (2012) 283–290.
[18] M. Ventura, O.C. Boerman, C. de Korte, M. Rijpkema, A. Heerschap, E. Oosterwijk, J.A. Jansen, X.F. Walboomers, Preclinical imaging in bone tissue engineering, Tissue Eng. Part B Rev. 20 (2014) 578–595.
[19] P.S. Lienemann, S. Metzger, A.S. Kivelio, A. Blanc, P. Papageorgiou, A. Astolfo, B.R. Pinzer, P. Cinelli, F.E. Weber, R. Schibli, M. Behe, M. Ehrbar, Longitudinal in vivo evaluation of bone regeneration by combined measurement of multi-pinhole SPECT and micro-CT for tissue engineering, Sci. Rep. 5 (2015) 10238.
[20] W.M. Hunter, F.C. Greenwood, Preparation of iodine-131 labelled human growth hormone of high specific activity, Nature 194 (1962) 495–496.
[21] S. Piskounova, R. Rojas, K. Bergman, J. Hilborn, The effect of mixing on the mechanical properties of Hyaluronan-based injectable hydrogels, Macromol. Mater. Eng. 296 (2011) 944–951.
[22] S. Stenfelt, G. Hulsart-Billstrom, L. Gedda, K. Bergman, J. Hilborn, S. Larsson, T. Bowden, Pre-incubation of chemically crosslinked hyaluronan-based hydrogels, loaded with BMP-2 and hydroxyapatite, and its effect on ectopic bone formation, J. Mater. Sci. Mater. Med. 25 (2014) 1013–1023.
[23] T.A. Einhorn, J.M. Lane, A.H. Burstein, C.R. Kopman, V.J. Vigorita, The healing of segmental bone defects induced by demineralized bone matrix. A radiographic and biomechanical study, J. Bone Joint Surg. Am. 66 (1984) 274–279.
[24] K. Bergman, T. Engstrand, J. Hilborn, D. Ossipov, S. Piskounova, T. Bowden, Injectable cell-free template for bone-tissue formation, J. Biomed. Mater. Res. A 91 (2009) 1111–1118.
[25] A.C. Docherty-Skogh, K. Bergman, M.J. Waern, S. Ekman, K. Hultenby, D. Ossipov, J. Hilborn, T. Bowden, T. Engstrand, Bone morphogenetic protein-2 delivered by hyaluronan-based hydrogel induces massive bone formation and healing of cranial defects in minipigs, Plast. Reconstr. Surg. 125 (2010) 1383–1392.
[26] L. Luca, A.L. Rougemont, B.H. Walpoth, R. Gurny, O. Jordan, The effects of carrier nature and pH on rhBMP-2-induced ectopic bone formation, J. Control. Release 147 (2010) 38–44.
[27] S. Piskounova, L. Gedda, G. Hulsart-Billstrom, J. Hilborn, T. Bowden, Characterization of recombinant human bone morphogenetic protein-2 delivery from injectable hyaluronan-based hydrogels by means of 125I-radiolabelling, J. Tissue Eng. Regen. Med. 8 (2014) 821–830.
[28] A. Docherty-Skogh, K. Bergman, M. Waern, S. Ekman, K. Hultenby, D. Ossipov, J. Hilborn, T. Bowden, T. Engstrand, Bone morphogenetic protein-2 delivered by hyaluronan-based hydrogel induces massive bone formation and healing of cranial defects in minipigs, Plast. Reconstr. Surg. 125 (2010) 1383–1392.
[29] A.C. Skogh, L. Kihlstrom, E. Neovius, C. Persson, M.O. Beckman, T. Engstrand, Variation in calvarial bone healing capacity: a clinical study on the effects of BMP-2-hydrogel or bone autograft treatments at different cranial locations, J. Craniofac. Surg. 24 (2013) 339–343.
[30] G. Hulsart-Billstrom, K. Bergman, B. Andersson, J. Hilborn, S. Larsson, K.B. Jonsson, A uni-cortical femoral defect model in the rat: evaluation using injectable hyaluronan hydrogel as a carrier for bone morphogenetic protein-2, J. Tissue Eng. Regen. Med. 9 (2015) 799–807.
[31] T.C. Laurent, J.R. Fraser, Hyaluronan, FASEB J. 6 (1992) 2397–2404.
[32] J.R. Fraser, T.C. Laurent, U.B. Laurent, Hyaluronan: its nature, distribution, functions and turnover, J. Intern. Med. 242 (1997) 27–33.
[33] V. Chappuis, L. Gamer, K. Cox, J.W. Lowery, D.D. Bosshardt, V. Rosen, Periosteal BMP2 activity drives bone graft healing, Bone 51 (2012) 800–809.
[34] G. Bhakta, B. Rai, Z.X. Lim, J.H. Hui, G.S. Stein, A.J. van Wijnen, V. Nurcombe, G.D. Prestwich, S.M. Cool, Hyaluronic acid-based hydrogels functionalized with heparin that support controlled release of bioactive BMP-2, Biomaterials 33 (2012) 6113–6122.
[35] G. Bhakta, Z.X. Lim, B. Rai, T. Lin, J.H. Hui, G.D. Prestwich, A.J. van Wijnen, V. Nurcombe, S.M. Cool, The influence of collagen and hyaluronan matrices on the delivery and bioactivity of bone morphogenetic protein-2 and ectopic bone formation, Acta Biomater. 9 (2013) 9098–9106.
[36] R. Marsell, B. Steen, M.V. Bais, D.P. Mortlock, T.A. Einhorn, L.C. Gerstenfeld, Skeletal trauma generates systemic BMP2 activation that is temporally related to the mobilization of CD73+ cells, J. Orthop. Res. 32 (2014) 17–23.
[37] J. Li, M.A. Miller, G.D. Hutchins, D.B. Burr, Imaging bone microdamage in vivo with positron emission tomography, Bone 37 (2005) 819–824.
[38] S. Toegel, O. Hoffmann, W. Wadsak, D. Ettlinger, L.K. Mien, K. Wiesner, J. Nguemo, H. Viernstein, K. Kletter, R. Dudczak, M. Mitterhauser, Uptake of bone-seekers is solely associated with mineralisation! A study with 99mTc-MDP, 153Sm-EDTMP and 18F-fluoride on osteoblasts, Eur. J. Nucl. Med. Mol. Imaging 33 (2006) 491–494.
[39] M.L. Frost, M. Siddique, G.M. Blake, A.E. Moore, P.J. Schleyer, J.T. Dunn, E.J. Somer, P.K. Marsden, R. Eastell, I. Fogelman, Differential effects of teriparatide on regional bone formation using (18)F-fluoride positron emission tomography, J. Bone Miner. Res. 26 (2011) 1002–1011.
[40] R.Z. Legeros, Calcium phosphate-based osteoinductive materials, Chem. Rev. 108 (2008) 4742–4753.
[41] E.T. Everett, Fluoride's effects on the formation of teeth and bones, and the influence of genetics, J. Dent. Res. 90 (2011) 552–560.
[42] M.D. Grynpas, E. Hamilton, R. Cheung, Y. Tsouderos, P. Deloffre, M. Hott, P.J. Marie, Strontium increases vertebral bone volume in rats at a low dose that does not induce detectable mineralization defect, Bone 18 (1996) 253–259.
[43] S. Takahashi, M. Sugimoto, Y. Kotoura, K. Sasai, M. Oka, T. Yamamuro, Long-term changes in the haversian systems following high-dose irradiation. An ultrastructural and quantitative histomorphological study, J. Bone Joint Surg. Am. 76 (1994) 722–738.
[44] R.J. Klinck, G.M. Campbell, S.K. Boyd, Radiation effects on bone architecture in mice and rats resulting from in vivo micro-computed tomography scanning, Med. Eng. Phys. 30 (2008) 888–895.
[45] K. Laperre, M. Depypere, N. van Gastel, S. Torrekens, K. Moermans, R. Bogaerts, F. Maes, G. Carmeliet, Development of micro-CT protocols for in vivo follow-up of mouse bone architecture without major radiation side effects, Bone 49 (2011) 613–622.
[46] W.M.S. Russell, R.L. Burch, The Principles of Humane Experimental Technique, Methuen, London, 1959.
[47] S. Kootala, Y. Zhang, S. Ghalib, V. Tolmachev, J. Hilborn, D.A. Ossipov, Control of growth factor binding and release in bisphosphonate functionalized hydrogels guides rapid differentiation of precursor cells in vitro, Biomater. Sci. 4 (2016) 250–254.